# Lateral transport of soil carbon and land–atmosphere $CO_2$ flux induced by water erosion in China

Yao Yue[a,b], Jinren Ni[a,1], Philippe Ciais[c], Shilong Piao[d,e,f], Tao Wang[e,f], Mengtian Huang[d], Alistair G. L. Borthwick[g], Tianhong Li[a], Yichu Wang[a], Adrian Chappell[h], and Kristof Van Oost[i]

[a]The Key Laboratory of Water and Sediment Sciences, Ministry of Education, College of Environmental Sciences and Engineering, Peking University, Beijing 100871, People's Republic of China; [b]School of Water Resources and Hydropower Engineering, Wuhan University, Wuhan 430072, People's Republic of China; [c]Laboratoire des Sciences du Climat et de l'Environnement, Institut Pierre Simon Laplace, Commissariat à l'Énergie Atomique et aux Ènergies Alternatives, CNRS, Université de Versailles Saint-Quentin-en-Yvelines, 91191 Gif-sur-Yvette, France; [d]Department of Ecology, Peking University, Beijing 100871, People's Republic of China; [e]Key Laboratory of Alpine Ecology and Biodiversity, Institute of Tibetan Plateau Research, Chinese Academy of Sciences, Beijing 100101, People's Republic of China; [f]CAS Center for Excellence in Tibetan Plateau Earth Sciences, Chinese Academy of Sciences, Beijing 100101, People's Republic of China; [g]School of Engineering, The University of Edinburgh, Edinburgh EH9 3JL, United Kingdom; [h]Land & Water, Commonwealth Scientific and Industrial Research Organisation, Canberra, ACT 2601, Australia; and [i]Earth and Life Institute, Georges Lemaître Centre for Earth and Climate Research, Université Catholique de Louvain, B-1348 Louvain, Belgium

Soil erosion by water impacts soil organic carbon stocks and alters $CO_2$ fluxes exchanged with the atmosphere. The role of erosion as a net sink or source of atmospheric $CO_2$ remains highly debated, and little information is available at scales larger than small catchments or regions. This study attempts to quantify the lateral transport of soil carbon and consequent land–atmosphere $CO_2$ fluxes at the scale of China, where severe erosion has occurred for several decades. Based on the distribution of soil erosion rates derived from detailed national surveys and soil carbon inventories, here we show that water erosion in China displaced $180 \pm 80$ Mt C·y$^{-1}$ of soil organic carbon during the last two decades, and this resulted a net land sink for atmospheric $CO_2$ of $45 \pm 25$ Mt C·y$^{-1}$, equivalent to 8–37% of the terrestrial carbon sink previously assessed in China. Interestingly, the "hotspots," largely distributed in mountainous regions in the most intensive sink areas (>40 g C·m$^{-2}$·y$^{-1}$), occupy only 1.5% of the total area suffering water erosion, but contribute 19.3% to the national erosion-induced $CO_2$ sink. The erosion-induced $CO_2$ sink underwent a remarkable reduction of about 16% from the middle 1990s to the early 2010s, due to diminishing erosion after the implementation of large-scale soil conservation programs. These findings demonstrate the necessity of including erosion-induced $CO_2$ in the terrestrial budget, hence reducing the level of uncertainty.

land–atmosphere $CO_2$ flux | soil carbon displacement | water erosion | national scale

Terrestrial ecosystems are a net sink of anthropogenic $CO_2$ globally (1, 2) but can be net sources or sinks regionally [e.g., Northeast Region of China (3)]. Knowledge of the distribution, magnitude, and variability of land carbon fluxes and underlying processes is important both for improving model-based projections of the carbon cycle and for designing ecosystem management options that effectively preserve carbon stocks and enhance carbon sinks. Despite considerable efforts made by the research community, the mechanisms governing uptake or release of carbon from land ecosystems are still poorly quantified (4).

Soil erosion occurs naturally but is accelerated by human cultivation of the landscape, and modifies $CO_2$ exchange (5) between the soil and atmosphere. Soil erosion destroys the physical protection of carbon in soil aggregates and accelerates decomposition, inducing a net $CO_2$ source. Continuous erosion over a long period can destabilize carbon in deeper soil horizons and trigger its decomposition e.g., as conditions of temperature and moisture become more favorable (6, 7). Soil erosion also decreases nutrient availability and reduces soil water holding capacity, affecting ecosystem productivity (8) with feedback to the ecosystem carbon balance. However, because only a fraction of eroded carbon is lost to the atmosphere, the rest may be lost to streams and rivers and eventually delivered to marine ecosystems or deposited in the landscape. With the fine and light soil particles preferentially delivered and associated with local minerals, carbon becomes more stable in the depositional area. Moreover, susceptibility and activation energy of organic matter also alter due to changes in the pH and redox conditions of the depositional environment, especially after a flood event. Hence, the decomposition rate is slower for microbial decomposition in the original soil profile, and carbon can be stored in deposition areas (9, 10). Finally, if productivity does not collapse due to soil fertility loss, carbon lost through soil erosion dynamic replacement may get replenished by litterfall, which creates a compensatory sink of atmospheric $CO_2$ (11, 12). This sink is called hereafter the dynamic replacement. To assess the net land–atmosphere $CO_2$ flux resulting from erosion, the sum of these sources and sinks must be quantified separately using a consistent framework.

Limited data from field measurements and model outputs for small watersheds (0.1–800 km$^2$) have suggested that the overall result of these water erosion processes is a net $CO_2$ sink (11, 13–16), with rate in the range 3–60 g C·m$^{-2}$·y$^{-1}$. These estimates were based on a small set of watersheds that were not necessarily representative of all of the regions impacted by erosion. The balance between decomposition and deposition can be inferred from measurements (usually $^{137}$Cs and C in soil profiles of representative landscape elements) at the scale of small watersheds (11), but estimates over larger regions must be drawn from mechanistic models and field surveys.

## Significance

The role of soil erosion as a net sink or source of atmospheric $CO_2$ remains highly debated. This work quantifies national-scale land–atmosphere $CO_2$ fluxes induced by soil erosion. Severe water erosion in China has caused displacement of $180 \pm 80$ Mt C·y$^{-1}$ of soil organic carbon during the last two decades, and the consequent land–atmosphere $CO_2$ flux from water erosion is a net $CO_2$ sink of $45 \pm 25$ Mt C·y$^{-1}$, equivalent to 8–37% of the terrestrial carbon sink previously assessed in China. This closes an important gap concerning large-scale estimation of lateral and vertical $CO_2$ fluxes from water erosion and highlights the importance of reducing uncertainty in assessing terrestrial carbon balance.

EARTH, ATMOSPHERIC, AND PLANETARY SCIENCES

The carbon balance of soils in China is impacted by soil erosion in many regions (17, 18). The aim here is to quantify the horizontal carbon transport induced by water erosion and consequent land−atmosphere $CO_2$ fluxes in China during the last ~20 y. The case of China is an interesting "natural experiment" because of severe erosion in the 1980s, which was reduced substantially after implementation of national large-scale soil conservation programs in the 1990s (19).

## Results

China occupies a large area of about 9.6 million square kilometers located within 73°33′E–135°05′E and 3°51′N–53°33′N. Its landforms range from deserts and plains to mountains, and its average land elevation varies from 3,000 m above sea level in Tibet to 10 m above sea level in the coastal region, roughly forming three steps from the west to the east. China covers several different climatic zones, and experiences annual precipitation varying from less than 400 mm in the dry area in the northwest to 2,000 mm in the southmost region. Consequently, China experiences very complicated soil erosion processes, of which the water-induced soil erosion is the most widely distributed. To estimate the carbon balance changes due to water erosion, we first give an overall picture of soil erosion and conservation based on the two national survey datasets of soil erosion in 1995–1996 and 2010–2012 (*SI Appendix, National Survey on Soil Erosion* and cese.pku.edu.cn/chinaerosion/). Then, by combining erosion rates with soil carbon samples collected at 8,980 sampling locations for all soil types (20) (*SI Appendix, Vertical Distribution of Soil Organic Carbon* and globalchange.bnu.edu.cn/research/soil2*), five erosion-related C flux components are quantified. As illustrated in Fig. 1, F1 is the removal of carbon from eroded soils, F2 is the deposition of eroded soil carbon, F3 is the dynamic replacement of atmospheric $CO_2$ in eroded soils, F4 is the carbon source to the atmosphere due to the decomposition of buried carbon, and F5 is the $CO_2$ source to the atmosphere from the decomposition of carbon during transport. F3 − (F4 + F5) constitutes the net land−atmosphere $CO_2$ flux from erosion; F1 and F2 represent components of the horizontal displacement of carbon.

**Soil Erosion and Conservation in China.** Fig. 2 *A* and *B* shows the distributions over China of mean erosion rate and the change in erosion rate determined from the two national surveys (the second national survey was carried out in 1995–1996, and the fourth national survey was carried out in 2010–2012) that combined remote sensing land cover imaging with field data (recorded in 68,155 survey units covering 1% of the total area experiencing water erosion; for details of land cover, precipitation and soil distribution, see *SI Appendix, Data*). The most fragile soils in China are

Mollisol, Calcic Inceptisols, and Ultisols based on the US Department of Agriculture (USDA) soil taxonomy [and Phaeozems, Calcic Cambisols, and Planosol based on Food and Agriculture Organization (FAO) soil classification]. As shown in Fig. 2*A*, the most intensively eroded regions are in the Loess Plateau region (mean rate of $3.0 \pm 1.2$ mm·y$^{-1}$ and soil removal $1.59 \pm 0.59$ Gt·y$^{-1}$, comprising 30.1% of the total) and in the upper Yangtze River Basin (mean rate $2.6 \pm 1.0$ mm·y$^{-1}$ and total soil removal $1.37 \pm 0.53$ Gt·y$^{-1}$, comprising 25.9% of the total), both of which have soils composed of readily eroded Inceptisols, based on USDA soil taxonomy [or Cambisols, based on FAO soil classification (21)], heavy rainfall events during the wet season (22), and intensive agriculture (23). Classified according to the water erosion grade, the histogram in Fig. 2*A*, *Inset*, shows that soil removal in Grade 3 areas (i.e., erosion rate = 1.90–3.70 mm·y$^{-1}$) contributes the most to total soil loss ($1.8 \pm 0.6$ Gt·y$^{-1}$, taking $34 \pm 11$% of the total), whereas Grade 2 areas (erosion rate = 0.74–1.90 mm·y$^{-1}$) comprise the largest proportion of the total erosional area (760,908 km$^2$, i.e., 50% of the total). After 1990, a huge national-scale program of "returning farmland to forests and grassland" for soil conservation and restoration was implemented in China, especially in the Loess plateau regions. About 22% of the total eroded area was put into restoration, mainly through soil conservation and afforestation projects. Hydraulic engineering works such as terracing, check dams, cisterns, and shelterbelts affected an area of about 1 million square kilometers during 2002–2012. Restrictions on forest litter raking and grazing in mountainous regions were further implemented over 0.75 million square kilometers during the same period (24) in North China (including the Loess Plateau) and Southwest China (including the upper Yangtze River). The histogram in Fig. 2*B*, *Inset*, shows that the combined area of Grades 2, 3, and 4 erosion (erosion rates = 0.74–0.90 mm·y$^{-1}$, 1.90–3.70 mm·y$^{-1}$, and 3.70–5.90 mm·y$^{-1}$, respectively) was reduced by 461,000 km$^2$ (i.e., reduction of $1.3 \pm 0.6$ Gt·y$^{-1}$ in soil removal). However, the combined area of Grades 5 and 6 erosion (erosion rate = 5.90–11.10 mm·y$^{-1}$, and erosion rate > 11.10 mm·y$^{-1}$, respectively) increased by 25,000 km$^2$ (i.e., increase of $0.3 \pm 0.1$ Gt·y$^{-1}$ in soil removal). The largest reduction of soil erosion in between the time periods covered by the two national surveys occurred in the Loess Plateau, where the erosion rate was reduced by $0.8 \pm 0.2$ mm·y$^{-1}$, and the total removal of soil was reduced by $1.1 \pm 0.4$ Gt·y$^{-1}$. Conversely, the rates of erosion continued to increase in 345 out of 378 counties in Northeastern and Southern China by 0.6 Gt·y$^{-1}$, with a 43.6% increase in erosional area in these two regions.

**Flux of Soil Carbon Removal.** The flux component associated with removal of soil carbon by erosion (F1; *SI Appendix*, Table S1),
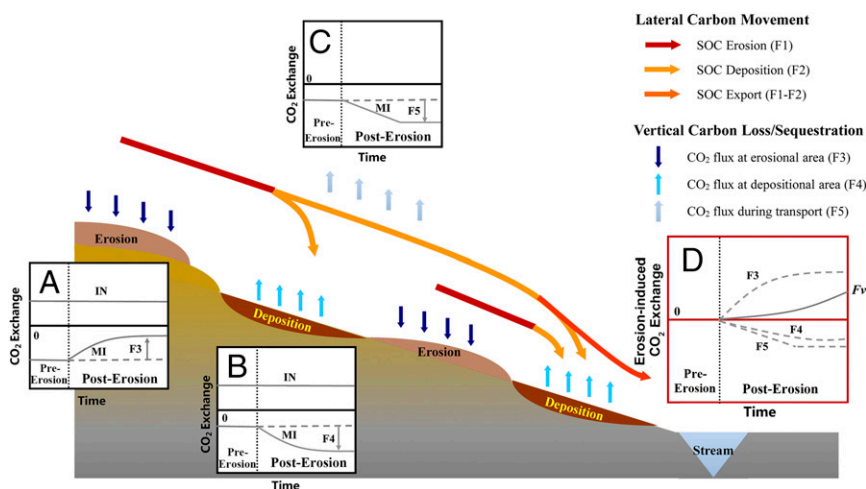


**Fig. 1.** Schematic of lateral and vertical carbon flux components under the impact of water erosion, transport and deposition areas. *Insets A, B,* and *C* demonstrate carbon input (IN) and carbon mineralization (MI) preerosion and posterosion; positive value represents carbon sink; *Inset D* shows the extra $CO_2$ flux induced by erosion in terms of the difference of (IN-MI) pre- and posterosion; *Fv* is the integrated results of F3, F4, and F5.

obtained by multiplying soil organic carbon (SOC) content from inventories by erosion rate, amounts to a total of $180 \pm 80$ Mt C·y$^{-1}$ over the last two decades. This removal flux is higher in regions with intensive erosion and high initial SOC densities (see Fig. 3$A$). The upper Yangtze River region, with average F1 of $140 \pm 63$ g C·m$^{-2}$·y$^{-1}$ for an eroded area of 367,525 km$^2$, contributes 29% to the total removal carbon, whereas North China has a smaller removal rate of $75 \pm 35$ g C·m$^{-2}$·y$^{-1}$ despite very severe erosion since the early 1950s (25). This decoupling between carbon removal and erosion rate is explained by the relatively low initial soil carbon content of North China (26). The histogram in Fig. 3$A$, *Inset*, shows that F1 in the erosional area of Grade 3 (erosion rate = 1.90–3.70 mm·y$^{-1}$) has the largest value ($79 \pm 25$ Mt C·y$^{-1}$). However, the SOC removal is most intensive ($469 \pm 156$ g C m$^{-2}$·y$^{-1}$) in areas that are Grade 6 (erosion rate > 11.10 mm·y$^{-1}$).

Between the two national surveys, F1 decreased by 44% ($64 \pm 28$ g C·m$^{-2}$·y$^{-1}$) due to the reduction of eroded areas. Fig. 3$B$ shows that F1 reduced by $80 \pm 36$ g C·m$^{-2}$·y$^{-1}$ in the combined area occupied by Inner Mongolia, North China, Northwest China, Southwest China, and where erosion slowed down (the total erosional area of the four regions reached 1,100,000 km$^2$), whereas F1 increased by $35 \pm 16$ g C·m$^{-2}$·y$^{-1}$ in Northeast and South China, where erosion intensified. The histogram in Fig. 3$B$, *Inset*, shows that F1 decreased by $127 \pm 50$ Mt C·y$^{-1}$ in the regions of water erosion Grades 2, 3, and 4 (erosion rates = 0.74–0.90 mm·y$^{-1}$, 1.90–3.70 mm·y$^{-1}$, and 3.70–5.90 mm·y$^{-1}$, respectively) but increased by $34 \pm 11$ Mt·y$^{-1}$ in Grades 5 and 6 regions (erosion rate = 5.90–11.10 mm·y$^{-1}$, and erosion rate > 11.10 mm·y$^{-1}$, respectively), mainly due to the corresponding changes in areas of each erosion grade.

**Flux of Soil Carbon Deposition.** The flux component representing deposition of eroded soil carbon (F2; *SI Appendix*, Table S1) was estimated from sediment delivery ratio (SDR) data. SDR is defined as the sediment yield at the outlet of a given small catchment and indicates the efficiency by which soil eroded in the catchment hillslopes is exported from the catchment. According to field data (22), SDR in the range 0.1–1 is positively correlated with erosion severity. Hence, typical nationwide SDR enables grading

according to the five classes of erosion severity and is applied to each of the 30,670 minimum polygons generated by the upscaling approach (*SI Appendix, Scale-up approach based on minimum polygons*). We derive F2 for the whole of China by summation over all polygons, giving a total F2 of $98 \pm 58$ Mt C·y$^{-1}$ averaged over the period between the two national surveys. The largest deposition rates are found for the Tibet Plateau, where the area affected by water erosion is only a small fraction of the total area ($199 \pm 118$ g C·m$^{-2}$·y$^{-1}$), followed by Northeast China ($90 \pm 53$ g C·m$^{-2}$·y$^{-1}$).

**Erosion-Induced CO$_2$ Flux in the Erosional Area.** Now we examine the effects of erosion on land–atmosphere CO$_2$ fluxes. The dynamic replacement flux component F3 is calculated using a modified method based on Van Oost et al. (11) that estimates the erosion-induced CO$_2$ flux in an area of interest by comparing the modeled SOC content (under the assumption that erosion induces no extra CO$_2$ flux) with the observed SOC content of a soil profile (*SI Appendix, Identifying the erosion-induced CO$_2$ fluxes*). The calculated rate of CO$_2$ uptake (*SI Appendix*, Table S1) is $32 \pm 16$ g C·m$^{-2}$·y$^{-1}$ nationwide, and the total dynamic replacement integrated across all eroded areas is $47 \pm 24$ Mt C·y$^{-1}$. Fig. 3$C$ shows that the spatial distribution of F3 is rather uniform across China, except for a few areas in Northeast, Northwest, and Southwest China that are CO$_2$ sources. Severely eroded areas in Southwest and North China (Fig. 2$A$) make the greatest contributions to the recovery CO$_2$ sink ($17.6 \pm 5.3$ Mt C·y$^{-1}$ and $9.5 \pm 6.6$ Mt C·y$^{-1}$, respectively).

Spatial distributions of decadal changes in the recovery CO$_2$ sink during the period between the two national surveys (Fig. 3$D$) and of the removal flux (Fig. 3$B$) are similar. This demonstrates that the acceleration or slowdown of horizontal carbon removal has changed the dynamic replacement in the same direction. For example, the dynamic replacement increased by $17 \pm 10$ g C·m$^{-2}$·y$^{-1}$ and $23 \pm 16$ g C·m$^{-2}$·y$^{-1}$ in Northeast and South China, where soil erosion accelerated during the period between the two national surveys. Meanwhile, the dynamic replacement weakened by $10 \pm 5$ g·m$^{-2}$·y$^{-1}$ in the Loess Plateau due to sustained soil conservation over the past ~20 y. Fig. 3$D$, *Inset*, also highlights a linear relationship between soil removal and F3 ($R^2 = 0.87$). Overall, the recovery CO$_2$ sink at

**Fig. 2.** Spatial distributions of water erosion in China from national surveys in 1995–1996 and 2010–2012. (*A*) Averaged erosion rate of the two surveys, where red lines demark boundaries of Loess Plateau and Upper Yangtze River Basin that suffer the most intensive water erosion. (*B*) Change in erosion rate during period between the two surveys, where red lines demark boundaries of regions in Northeast and South China that experience fastest increase in erosional area. *Insets* consist of histograms of (*A*) average and (*B*) change in total soil removal with superimposed black dots indicating water erosion area, classified according to water erosion grade.

the country scale decreased from $52 \pm 28$ Mt C·y$^{-1}$ in 1995–1996 to $42 \pm 21$ Mt C·y$^{-1}$ in 2010–2012, being primarily driven by effective soil conservation measures in China. Interestingly, the plot of accumulated F3 as a function of accumulated erosion area (defined as an area with water erosion rate larger than 0.74 mm·y$^{-1}$) in Fig. 3C, *Inset*, shows that the most intensive sink area (>40 g C·m$^{-2}$·y$^{-1}$) contributes 19.3% (9.1 Mt C·y$^{-1}$) to the national erosion-induced carbon sink while taking up only 1.5% of the total area undergoing water erosion. By contrast, the weakest sink area (<10 g C·m$^{-2}$·y$^{-1}$) contributes only 26% (12.2 Mt C·y$^{-1}$) of the total sink although it covers 79.3% of the erosional area. The largest rates of recovery CO$_2$ uptake are located in North and Southwest regions where erosion is still severe. This finding agrees with saturation theory that the most efficient uptake of CO$_2$ by a soil carbon pool occurs when it is farthest from carbon saturation (27).

It should be noted that the modified method based on Van Oost et al. (11) ignores dissolved losses of C from topsoil through leaching, which could contribute another source of vertical loss. As suggested by Li et al. (28), Long et al. (29), and Gou et al. (30), the dissolved organic carbon (DOC) leaching potential ranges from 3.8 to 8.7 kg·ha$^{-1}$, corresponding to a DOC leaching potential of 0.55–0.96 Mt C·y$^{-1}$. Li et al. (28) assumed that DOC leaching is linearly proportional to precipitation, and thus derived an empirical formula for leaching of hillslope croplands in a subcatchment of the Yangtze River basin. Using this alternative approach, the DOC leaching potential throughout China is estimated to be 0.94 Mt C·y$^{-1}$ using yearly averaged precipitation data for the period 1995−2012. These two sets of results show that the potential DOC leaching flux in China is negligible compared with F3.

**Erosion-Induced CO$_2$ Flux in the Depositional Area.** It is commonly accepted that deposition of carbon induces a CO$_2$ source in the depositional area (13, 31). As the eroded soil is deposited, part of the previous topsoil carbon enters into and enriches the first layer of subsoil (31). Decomposition of the newly buried carbon-rich soil brings about an extra CO$_2$ source. This flux component F4 was calculated as the product of deposited SOC (F2) by the decomposition rate of carbon in the subsoil layer, assuming an exponentially decreasing law of turnover rate with depth (*SI Appendix, Erosion-Induced CO$_2$ Source*), which yields an estimate of F4 in the range $0.6 \pm 0.4$ g C·m$^{-2}$, equivalent to a net CO$_2$ source to the atmosphere of $0.9 \pm 0.5$ Mt C·y$^{-1}$. Berhe et al. (32) found that the rate of decay of the most active soil C pool in a depositional landform located in naturally eroding grassland is far from exponentially declining. At or near steady state (for soil and C accumulation), the assumption of exponential decay should nevertheless be acceptable. However, at the timescales under consideration (decades), the buried SOC can effectively be preserved (e.g., refs. 11, 33, and 34), because the decay rates in burial zones are substantially lower than in topsoils for both steady and dynamic profiles. Thus, the physical environment is the key control, rather than the chemical nature of the SOC, and the approximation of an exponential law of decay is acceptable.

**Erosion-Induced CO$_2$ Flux During Sediment Transport.** By breaking down the soil aggregates and transporting soil material, erosion promotes carbon emission. Although Jacinthe et al. (35) found, in an incubation experiment, that a substantial fraction of SOC (20–50%) degraded into CO$_2$ after 100 d, other studies [e.g., Wang et al. (34) and Van Hemelryck (36)] reported that the additional release was hardly induced by erosion compared with the baseline condition of noneroding soil. Following Guenet et al. (37), who measured the enhanced emission when SOC enters the aquatic environment, we assumed that the rate of decomposition is ~63% higher during transport. As a result, we further derived the erosion-induced flux component during transport F5 to be a CO$_2$ source of $1 \pm 0.5$ Mt C·y$^{-1}$, which is relatively small compared with F3. The present approach is therefore consistent with the understanding of the impact of erosion on soil C decomposition rates on land.

## Discussion

**Importance and Comparison.** F1 represents 0.16% of the total 100–120 Gt C (38, 39) of SOC storage in China. Lal (7) derived the amount of soil erosion from sediment transport data collected from different basins worldwide. By assuming the SOC content to be 2–3%, Lal estimated that SOC removals in Europe and Oceania, each of which have a similar area to China, are 200–400 Mt·y$^{-1}$ and 100–200 Mt·y$^{-1}$, respectively; these values are comparable with F1 in China, where SOC content is 3.4%. However, Zhang et al. (40) calculated a much higher SOC erosion of 640–1,040 Mt C·y$^{-1}$ based on a much higher assessment of soil erosion (11.3–18.2 Gt·y$^{-1}$) than in the present study (3.2–7.4 Gt·y$^{-1}$). SOC deposition represents 55% of SOC removal flux in the same source catchment. Ratios of F2 to F1 averaged over Yangtze River Basin, Pearl River Basin, Huai River, and Yongding River Basin agree well with values obtained in a previous study (41), whereas those of the Yellow River Basin and Liao River Basin are higher. An important sink of carbon is SOC exported from the source watersheds that enters into the aquatic environment (42, 43), and that can be determined from subtracting the terrestrial deposition from the SOC removal (F1 – F2). It can be seen that total SOC exported from source catchments is $82 \pm 49$ Mt C·y$^{-1}$ (*SI Appendix*, Table S1), which represents roughly half of the total SOC eroded inland. This implies that the potential aquatic carbon sink in China can be significant. Of all of the regions, the Southwest contributes most to total SOC exported from source watersheds ($28 \pm 16$ Mt C·y$^{-1}$). In particular, SOC that is finally delivered to the ocean comprises a more permanent sink. The particulate organic carbon (POC) fluxes at the outlets of seven major river basins in China, whose combined drainage area is ~76% of the total external drainage area of China, imply that the burial of carbon with sediment from these rivers sums up to 5.4 Mt C·y$^{-1}$ (*SI Appendix*, Table S2).

Averaged over the total area suffering water erosion, F3 is 33 g C·m$^{-2}$·y$^{-1}$, roughly within the range of 0.7–60 g C·m$^{-2}$·y$^{-1}$ obtained from field estimates for small watersheds in Europe and North America (11, 13, 44–46). It is important to note that the recovery CO$_2$ sink is smaller than the horizontal removal of carbon (F1). The average ratio of vertical F3 to F1 (vertical to lateral carbon ratio, VLC) in eroding areas is ~0.25, approximately comparable with Van Oost et al.'s (11) value of 0.26 estimated for representative small watersheds in Europe and extrapolated to global scale. In China, lower VLC ratios occur in the Tibetan Plateau (~0.05), Northwest China (~0.12), and Inner Mongolia (~0.17), where the water erosion area is limited. Conversely, higher VLC ratios are found in North China (~0.51) and Southwest regions (~0.34) subject to intensive water erosion. This also implies an increasing trend of erosion-induced recovery CO$_2$ sink in the Northeast and the Southeast regions, noting their relatively high VLC ratios and increasing trend of SOC removal during the past 20 y. The average ratio of dynamic replacement to SOC removal obtained in the present study for China is 0.25; hence, we estimate the magnitude of the global recovery CO$_2$ sink to be on the order of 0.1–0.4 Gt C·y$^{-1}$ (the global SOC flux having previously been estimated to be 0.4–1.6 Gt C·y$^{-1}$) (11, 47, 48). In other words, erosion-induced CO$_2$ sequestration could contribute 5–20% to the global land sink.

Compared with the erosion-induced CO$_2$ sink in the erosional area, the enhanced CO$_2$ emissions in the depositional area or during sediment transport are relatively small, together representing ~4% of F3. Therefore, the total vertical C flux obtained by summing up F3, F4, and F5 equates to a CO$_2$ sink of $45 \pm 25$ Mt C·y$^{-1}$ (*SI Appendix*, Table S1), taking up 8–37% of the total terrestrial CO$_2$ sink of China (0.19–0.26 Gt C·y$^{-1}$) (3).

**Control of Carbon Flux.** A sharp decrease in SOC removal occurred over the past ~20 y, which may be mainly attributed to the large reduction in soil erosion resulting from conservation activities and climate change. Miao et al. (49) suggested that climate change
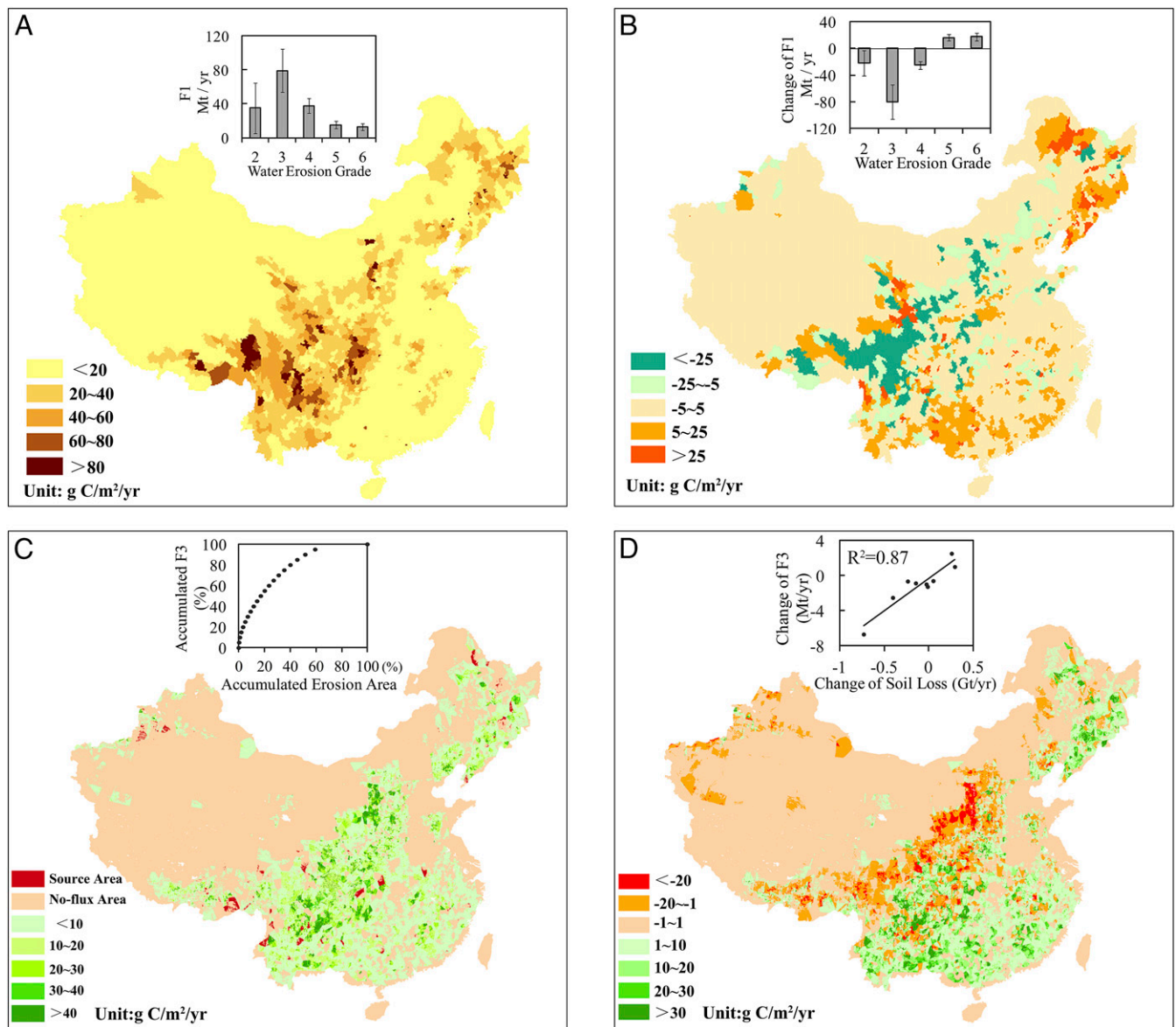
**Fig. 3.** Spatial distributions of water erosion-induced carbon fluxes in China from national surveys in 1995–1996 and 2010–2012. (*A*) Averaged F1 from the two surveys, (*B*) change in F1 during the period between the two surveys, (*C*) averaged F3, and (*D*) change in F3. *Insets* comprise (*A*) histogram of averaged F1 and (*B*) histogram of change in F1 during the period between the two surveys, classified according to water erosion grade; (*C*) plot of accumulated F3 with erosional area; and (*D*) scatter plot of change in F3 as a function of change in soil loss during the period between the two surveys, with regression line superimposed.

contributed 17% and 48% to the decrease of sediment yield in the upper and middle reaches, respectively, of Yellow River Basin, whereas conservation activities contributed 83% and 52% from 1958 to 2008. This implies that China's conservation policy has proved very efficient in controlling soil loss. The reduced soil erosion also caused the erosion-induced $CO_2$ sink to diminish in the erosional area (F3). A sensitivity analysis carried out by altering each parameter by ±20% (*SI Appendix, Uncertainty and Sensitivity Analysis*) shows that carbon input (±29%) is the primary factor determining the $CO_2$ sink, followed by erosion rate (±23%) and carbon turnover rate (±13%). To further diagnose the influences of various drivers that have not been included in the model calculation, we performed multiple linear regression of F3 over all land polygons as a function of vegetation type, annual precipitation, and average temperature. The results show that the spatial variation of F3 is primarily driven by the average temperature (18.8%), which controls the key parameter of net primary production (NPP) through affecting the enzyme

kinetics during the processes of photosynthesis and autotrophic respiration (50, 51), and is secondarily driven by precipitation and vegetation types. The most sensitive regions, which are small in area but contribute a great amount to both lateral and vertical C fluxes, are hotspots on which conservation policies should be focused.

## Conclusions

In summary, our results show that water erosion removed $180 \pm 80$ Mt C·y$^{-1}$ of soil carbon in China over the last two decades, which caused a redistribution of land−atmosphere $CO_2$ fluxes. The erosion-induced $CO_2$ sequestration is about 8–37% of the terrestrial carbon sink at country scale. According to the average ratio of dynamic replacement to SOC removal obtained in this study for China (0.25), we extrapolate that erosion-induced $CO_2$ sequestration could contribute 5–20% of the global land sink. These results confirm the significance of lateral soil carbon transport by erosion processes in the global carbon cycle, and

highlight the importance of reducing uncertainty in assessing the terrestrial carbon balance due to soil erosion.

## Methods

The lateral and vertical carbon fluxes induced by water erosion of soils are calculated based on national surveys (carried out in 1995–1996 and 2010–2012) on erosion rates and a national soil database containing 8,980 profiles, together with NPP and carbon pool turnover rate data derived from 10 global carbon cycle models. Furthermore, multiple regression analysis is undertaken based on long series datasets on distributions of vegetation cover and climatic information (1995–2012) obtained from 675 gauging stations located throughout China.

Estimates of lateral SOC fluxes of erosion (F1), deposition (F2), and the dynamic replacement at the erosional area (F3) were determined based on minimum polygons generated by overlaying the data layers of erosion rate, soil carbon content, NPP, and carbon pool turnover rate in ArcGIS. F1 was given by the product of erosion rate and SOC content in the eroded soil (*SI Appendix, SOC erosion*). F2 was determined by introducing the concept of sediment delivery ratio (*SI Appendix, SOC deposition*). F3 was assessed using a modified model based on Van Oost et al.'s method (11) (*SI Appendix, Carbon Recovery at the Eroded Area*). These three fluxes were calculated and their values added up for

each polygon, and the total flux at country scale was obtained by summation over all polygons (*SI Appendix, Scale-up approach based on minimum polygons*).

Erosion-induced $CO_2$ flux at the depositional area (F4) was estimated as the $CO_2$ emission from the newly buried carbon-rich topsoil (*SI Appendix, Erosion-Induced $CO_2$ Source*). Erosion-induced $CO_2$ flux during sediment transport (F5) was determined as the difference between $CO_2$ emissions before and after erosion (*SI Appendix, Enhanced Decomposition of SOC*).

1. Le Quéré C, et al. (2009) Trends in the sources and sinks of carbon dioxide. *Nat Geosci* 2:831–836.
2. Intergovernmental Panel on Climate Change (2013) *Climate Change 2013: The Physical Science Basis. Contribution of Working Group I to the Fifth Assessment Report of the Intergovernmental Panel on Climate Change*, eds Stocker TF, et al. (Cambridge Univ Press, New York).
3. Piao S, et al. (2009) The carbon balance of terrestrial ecosystems in China. *Nature* 458(7241):1009–1013.
4. Intergovernmental Panel on Climate Change (2014) *Climate Change 2014: Synthesis Report. Contribution of Working Groups I, II and III to the Fifth Assessment Report of the Intergovernmental Panel on Climate Change*, eds Pachauri RK, et al. (Intergov Panel Clim Change, Geneva).
5. Berhe AA, Harte J, Harden JW, Torn MS (2007) The significance of the erosion-induced terrestrial carbon sink. *Bioscience* 57(4):337–346.
6. Jacinthe PA, Lal R (2001) A mass balance approach to assess carbon dioxide evolution during erosional events. *Land Degrad Dev* 12(4):329–339.
7. Lal R (2003) Soil erosion and the global carbon budget. *Environ Int* 29(4):437–450.
8. Fontaine S, et al. (2007) Stability of organic carbon in deep soil layers controlled by fresh carbon supply. *Nature* 450(7167):277–280.
9. Doetterl S, et al. (2016) Erosion, deposition and soil carbon: A review of process-level controls, experimental tools and models to address C cycling in dynamic landscapes. *Earth Sci Rev* 154:102–122.
10. Berhe AA, Kleber M (2013) Erosion, deposition, and the persistence of soil organic matter: Mechanistic considerations and problems with terminology. *Earth Surf Processes Landforms* 38(8):908–912.
11. Van Oost K, et al. (2007) The impact of agricultural soil erosion on the global carbon cycle. *Science* 318(5850):626–629.
12. Kirkels FMSA, Cammeraat LH, Kuhn NJ (2014) The fate of soil organic carbon upon erosion, transport and deposition in agricultural landscapes—A review of different concepts. *Geomorphology* 226:94–105.
13. Liu S, Bliss N, Sundquist E, Huntington TG (2003) Modeling carbon dynamics in vegetation and soil under the impact of soil erosion and deposition. *Global Biogeochem Cycles* 17(2):1074–1097.
14. Renwick WH, Smith SV, Sleezer RO, Buddemeier RW (2004) Comment on "Managing soil carbon" (II). *Science* 305(5690):1567, and author reply (2004) 305(5690):1567.
15. Harden JW, et al. (2008) Soil erosion: Data say C sink. *Science* 320(5873):178–179.
16. Quinton JN, Govers G, Van Oost K, Bardgett RD (2010) The impact of agricultural soil erosion on biogeochemical cycling. *Nat Geosci* 3:311–314.
17. Pan G, Xu XW, Smith P, Pan WN, Lal R (2010) An increase in topsoil SOC stock of China's croplands between 1985 and 2006 revealed by soil monitoring. *Agric Ecosyst Environ* 136(1-2):133–138.
18. Stacy EM, Hart SC, Hunsaker CT, Johnson DW, Berhe AA (2015) Soil carbon and nitrogen erosion in forested catchments: implications for erosion-induced terrestrial carbon sequestration. *Biogeosciences* 12(16):4861–4874.
19. Miao CY, Ni JR, Borthwick AGL (2010) Recent changes of water discharge and sediment load in the Yellow River basin, China. *Prog Phys Geogr* 34(4):541–561.
20. Shang Guan W, Dai YJ, Liu BY, Ye AZ, Yuan H (2012) A soil particle-size distribution dataset for regional land and climate modelling in China. *Geoderma* 171–172:85–91.
21. Shi XZ, et al. (2006) Cross-reference system for translating between genetic soil classification of China and soil taxonomy. *Soil Sci Soc Am J* 70(1):78–83.
22. Jing K, Wang WZ, Zheng FL (2005) *Soil Erosion and Environment in China* (Science Press, Beijing), Chinese.
23. Lal R (2002) Soil carbon sequestration in China through agricultural intensification, and restoration of degraded and desertified ecosystems. *Land Degrad Dev* 13(6):469–478.
24. Ministry of Water Resources PRC, National Bureau of Statistics PRC (2013) Bulletin of First National Census for Water (China Water & Power Press, Beijing).
25. Chen CQ (1992) Study on soil erosion using remote sensing technique in the Loess Plateau of the North Shaanxi Province. *XVIIth ISPRS Congress* (Int Soc Photogramm Remote Sens, Washington, DC), pp 137–141.
26. Wang YQ, Zhang XC, Zhang JL, Li SJ (2009) Spatial variability of soil organic carbon in a watershed on the Loess Plateau. *Pedosphere* 19(4):486–495.
27. Stewart CE, Paustian K, Conant RT, Plante AF, Six J (2007) Soil carbon saturation: Concept, evidence and evaluation. *Biogeochemistry* 86(1):19–31.
28. Li TK, Zhu B, Wang XG, Kou CL (2013) Characteristics of dissolved organic carbon leaching from hillslope cropland of purple soil in the Sichuan Basin, China. *J Food Agric Environ* 11(2):1522–1527.
29. Long GQ, Jiang YJ, Sun B (2015) Seasonal and inter-annual variation of leaching of dissolved organic carbon and nitrogen under long-term manure application in an acidic clay soil in subtropical China. *Soil Tillage Res* 146(Part B):270–278.
30. Gou XL, et al. (2013) Effect of changes in seasonal freeze-thaw pattern on DOC loss from leaching in the alpine forest soil. *J Soil Water Conserv* 27(6):205–210.
31. Van Oost K, et al. (2005) Landscape-scale modeling of carbon cycling under the impact of soil redistribution: The role of tillage erosion. *Global Biogeochem Cycles* 19(4):GB4014.
32. Berhe AA, Harden JW, Torn MS, Harte J (2008) Linking soil organic matter dynamics and erosion-induced terrestrial carbon sequestration at different landform positions. *J Geophys Res* 113(G4):4647–4664.
33. Van Oost K, et al. (2012) Legacy of human-induced C erosion and burial on soil-atmosphere C exchange. *Proc Natl Acad Sci USA* 109(47):19492–19497.
34. Wang Z, et al. (2014) The fate of buried organic carbon in colluvial soils: A long-term perspective. *Biogeosciences* 11(3):873–883.
35. Jacinthe PA, Lal R, Kimble JM (2001) Organic carbon storage and dynamics in croplands and terrestrial deposits as influenced by subsurface tile drainage. *Soil Sci* 166(5):322–335.
36. Van Hemelryck H, Govers G, Van Oost K, Merckx R (2010) The effect of soil redistribution on soil organic carbon: An experimental study. *Biogeosciences* 7(12):3971–3986.
37. Guenet B, et al. (2014) Fast mineralization of land-born C in inland waters: First experimental evidences of aquatic priming effect. *Hydrobiologia* 721(1):35–44.
38. Ni J (2001) Carbon storage in terrestrial ecosystems of China: Estimates at different spatial resolutions and their responses to climate change. *Clim Change* 49(3):339–358.
39. Ni J (2013) Carbon storage in Chinese terrestrial ecosystems: Approaching a more accurate estimate. *Clim Change* 119(3):905–917.
40. Zhang H, et al. (2014) Inclusion of soil carbon lateral movement alters terrestrial carbon budget in China. *Sci Rep* 4:7247.
41. Li ZG, Liu BZ (2006) Calculation on soil erosion amount of main river basin in China. *Sci Soil Water Conserv* 4(2):1–6.
42. Stallard RF (1998) Terrestrial sedimentation and the carbon cycle: Coupling weathering and erosion to carbon burial. *Global Biogeochem Cycles* 12(2):231–257.
43. Smith SV, Sleezer RO, Renwick WH, Buddemeier RW (2005) Fates of eroded soil organic carbon: Mississippi Basin case study. *Ecol Appl* 15(6):1929–1940.
44. Yoo K, et al. (2005) Erosion of upland hillslope soil organic carbon: Coupling field measurements with a sediment transport model. *Global Biogeochem Cycles* 19(3):1721–1730.
45. Harden JW, et al. (1999) Dynamic replacement and loss of soil carbon on eroding cropland. *Global Biogeochem Cycles* 13(4):885–901.
46. Billings SA, Buddemeier RW, Richter DD, Van Oost K, Bohling G (2010) A simple method for estimating the influence of eroding soil profiles on atmospheric $CO_2$. *Global Biogeochem Cycles* 24(2):1–14.
47. Ito A (2007) Simulated impacts of climate and land-cover change on soil erosion and implication for the carbon cycle. *Geophys Res Lett* 34(9):L09403.
48. Doetterl S, Van Oost K, Six J (2012) Towards constraining the magnitude of global agricultural sediment and soil organic carbon fluxes. *Earth Surf Processes Landforms* 37(6):642–655.
49. Miao CY, Ni JR, Borthwick AGL, Yang L (2011) A preliminary estimate of human and natural contributions to the changes in water discharge and sediment load in the Yellow River. *Global Planet Change* 76(3-4):196–205.
50. Bernacchi CJ, Singsaas EL, Pimentel C, Portis AR, Jr, Long SP (2001) Improved temperature response functions for models of Rubisco-limited photosynthesis. *Plant Cell Environ* 24(2):253–259.
51. Song WM, et al. (2015) Simulated rain addition modifies diurnal patterns and temperature sensitivities of autotrophic and heterotrophic soil respiration in an arid desert ecosystem. *Soil Biol Biochem* 82:143–152.